

A multiscale analysis of nutrient transport and biological tissue growth *in vitro*

R. D. O'Dea^{1*}, M. R. Nelson^{1,2}, A. J. El Haj³, S. L. Waters⁴ & H. M. Byrne^{5,6}

¹ School of Mathematical Sciences, University of Nottingham
Nottingham, NG7 2RD, UK

² School of Science and Technology, Nottingham Trent University
Clifton Campus, Nottingham, NG11 8NS, UK

³ Institute for Science & Technology in Medicine, Keele University
Guy Hilton Research Centre, Stoke-on-Trent ST4 7QB, UK

⁴ Oxford Centre for Industrial and Applied Mathematics
Mathematical Institute, Andrew Wiles Building, Radcliffe Observatory Quarter,
Woodstock Road, Oxford, OX2 6GG, UK

⁵ Department of Computer Science, University of Oxford
Wolfson Building, Parks Road, Oxford, OX1 3QD, UK

⁶ Oxford Centre for Collaborative Applied Mathematics
Mathematical Institute, Andrew Wiles Building, Radcliffe Observatory Quarter,
Woodstock Road, Oxford, OX2 6GG, UK

In this paper, we consider the derivation of macroscopic equations appropriate to describe the growth of biological tissue, employing a multiple-scale homogenisation method to accommodate explicitly the influence of the underlying microscale structure of the material, and its evolution, on the macroscale dynamics. Such methods have been widely used to study porous and poroelastic materials; however, a distinguishing feature of biological tissue is its ability to remodel continuously in response to local environmental cues. Here, we present the derivation of a model broadly applicable to tissue engineering applications, characterised by cell proliferation and extracellular matrix deposition in porous scaffolds used within tissue culture systems, which we use to study coupling between fluid flow, nutrient transport and microscale tissue growth. Attention is restricted to surface accretion within a rigid porous medium saturated with a Newtonian fluid; coupling between the various dynamics is achieved by specifying the rate of microscale growth to be dependent upon the uptake of a generic diffusible nutrient. The resulting macroscale model comprises a Darcy-type equation governing fluid flow, with flow characteristics dictated by the assumed periodic microstructure and surface growth rate of the porous medium, coupled to an advection–reaction equation specifying the nutrient concentration. Illustrative numerical simulations are presented to indicate the influence of microscale growth on macroscale dynamics, and to highlight the importance of including experimentally-relevant microstructural information in order to correctly determine flow dynamics and nutrient delivery in tissue engineering applications.

Keywords: multiscale homogenisation, porous flow, tissue engineering

1. Introduction

Biological tissue growth is an extremely complex process, involving the interaction of a wide range of biological and biophysical factors, which span multiple spatial and temporal scales. It is becoming

*Corresponding author e-mail: reuben.o'dea@nottingham.ac.uk

accepted that complementary study of biological growth processes by both experimental and theoretical methods is required in order to improve our understanding of how observed phenomena are generated; realising this goal will impact on a wide range of experimental and clinical biomedical research, including *in vitro* tissue engineering. The latter refers to the creation of replacement tissues in a laboratory, with which to address the shortfall in donor tissue available for implantation into patients in the treatment of a wide range of conditions. While replacement skin grafts have been successfully produced in the laboratory and translated into the clinic (Horch *et al.*, 2007), the production of more complex replacement tissues and organs is not currently possible. An experimental paradigm for such studies entails seeding a biodegradable porous scaffold with cells; subsequent incubation within a culture medium-filled bioreactor allows the cells to colonise the porous scaffold (termed a tissue construct). On implantation, the degrading scaffold is replaced by extracellular materials such as collagen and proteoglycans, which are laid down by the cells (Freed *et al.*, 1994).

The importance of this field has spawned a plethora of experimental and theoretical studies, investigating various aspects of *in vitro* tissue growth and subsequent *in vivo* implantation; the diverse contributory processes (from intracellular signalling networks to tissue-level patterning and mechanics) has led theoretical investigators to apply myriad different mathematical modelling approaches. One class of theoretical models is those that aim to provide a description of the tissue construct appropriate at the macroscale (tissue-scale). Typically, such models comprise systems of partial differential equations describing (for example) the average culture medium flow characteristics, nutrient supply, cell density, or mechanical effects (Araujo & McElwain, 2005; Lemon *et al.*, 2006; Ambrosi *et al.*, 2010; O’Dea *et al.*, 2010). At the microscale, however, such models are not appropriate since they do not reflect the nature of individual cells, or the influence of tissue microstructure on system behaviour. The modelling literature regarding aspects of biological tissue dynamics at the scale of a single cell is extensive and varied; representative studies include: consideration of intracellular (Bridge *et al.*, 2010) and intercellular (Collier *et al.*, 1996; Webb & Owen, 2004) signalling processes and their influence on cell behaviour, within spatially discrete models comprising systems of ordinary differential equations; detailed analysis of the mechanical behaviour of individual cells via biophysical continuum models (Bathe *et al.*, 2002; Mack *et al.*, 2004); and lattice-free cellular automata-type modelling approaches, representing in detail the behaviour of small populations of cells (Meineke *et al.*, 2001; Van Leeuwen *et al.*, 2009).

The analysis of such cell-level models can be highly numerical in nature, and to represent realistically tissue-level dynamics requires very large numbers of cells, which provides significant computational challenges. The derivation of tissue-scale models accommodating aspects of cell-level detail, but within continuum formulations that may admit analytic progress or simpler numerical analysis, is therefore of great importance to the theoretical investigation of tissue growth. To address this, various multiscale (or homogenisation) techniques have been employed to derive macroscale models directly from underlying microscale systems, enabling some of the dynamics to be incorporated in a mathematically precise way. Representative examples employing this method in a biological context include: Turner *et al.* (2004) and Fozard *et al.* (2010), in which continuum representations of the collective motion of adherent epithelial cells were derived; O’Dea & King (2011, 2012), who showed that microscale patterns formed via discrete intercellular signalling mechanisms can be represented within reaction–diffusion systems; and Chapman *et al.* (2008), Shipley & Chapman (2010) and Marciniak-Czochra & Ptashnyk (2008), in which macroscale models for transport in biological tissues were considered. Many of these studies of homogenisation employ and extend methods from older studies of porous and poroelastic materials such as Burridge & Keller (1981) and Mei & Auriault (1991). Historically, the inspiration for many studies applying homogenisation theory includes the study of soil filtration – see, *e.g.*, Ptashnyk & Roose (2010); related applications include the plant sciences (Chavarría-Krauser & Ptashnyk, 2010);

Band & King, 2012).

A distinguishing feature of biological tissue is its ability to grow and adaptively remodel in response to local environmental conditions. While continuum models for growth and tissue remodeling abound (see *e.g.* Dervaux & Ben Amar (2008, 2010), Nelson *et al.* (2011, 2013); a comprehensive review is given in Humphrey (2003)), to our knowledge a macroscale description of growing tissues, obtained by homogenisation of microscale dynamics, does not exist. Here, we address this deficiency by considering nutrient-limited microscale growth. Specifically, we consider appositional growth (also termed accretion), whereby growth occurs via deposition of new material on the exterior of the growing tissue. This is distinct from the alternative process of interstitial growth, in which growth occurs throughout the tissue; such a process is problematic from a mathematical point of view since it leads to the genesis of residual stresses, which must be accommodated in a physically-reasonable way. We study an idealised representation of appositional growth within a rigid porous medium, in which growth of the solid phase results from a change of state from fluid to solid at the solid-fluid interface, this phase-change occurring at a prescribed rate, dependent on the local availability of a generic diffusible nutrient. Our model is therefore appropriate in the ‘thin-rim’ or ‘fast-consumption’ limit (King & Franks, 2007), and describes cell growth and extracellular matrix (ECM) deposition within tissue engineering scaffolds, such as those employed in perfusion bioreactors, or appositional bone tissue growth, *in vivo*. Furthermore, the multiscale analysis that we employ relies on the assumption that the material under consideration has a (locally) spatially-periodic microstructure. This homogenisation approach is widely used to describe flows within biological tissue (either explicitly such as in Shipley & Chapman (2010), or implicitly through its underpinning of macroscale porous flow models); however, the validity of its application to tissue growth in general is undermined by the disordered structure of many biological tissues. In such scenarios, its accuracy is influenced by the statistics of the tissue structure (and relevant model parameters); see, for example, Rubinstein & Torquato (1989) in which upper and lower bounds on the Darcy permeability are derived for a random porous medium, and Chernyavsky *et al.* (2011) in which convergence of the homogenisation approximation is considered in detail, in the context of placental transport. In such cases, the macroscale description that arises should not be viewed as an exact description, rather it provides an idealised framework that is amenable to analysis and provides insight into macroscale growth processes. Further, our study focusses on *in vitro* tissue engineering applications, for which scaffold manufacture can carefully be controlled — three-dimensional printing, stereo-lithography and fused deposition modelling, for example, constitute excellent methods for producing well-defined and regular scaffolds (see Hutmacher *et al.* (2004); Hollister (2005) and references therein) to which the assumption of structural regularity will apply.

On theoretical and, subsequently, biological grounds, we study our model in the limit for which growth is slow, and hence relegated to $\mathcal{O}(\varepsilon)$ in the multiple-scales analysis; however, our analysis reveals that such growth (and associated nutrient consumption) is evident nevertheless in the leading-order problem that we derive. In sum, this paper indicates that microscale surface growth may be incorporated into macroscale models in a straightforward way; additionally, we present illustrative numerical simulations and, via inclusion of experimental data detailing the microscale structure of a typical tissue engineering scaffold, highlight how micro- and macroscale flow characteristics in realistic scaffolds may differ from more idealised models. The results that we present indicate that these differences are likely to influence dramatically the transport of nutrients to cells seeded in such structures and hence should be accounted for in macroscale models seeking to provide a more realistic description of tissue dynamics.

The remainder of this paper is organised as follows. In §2, we summarise the equations governing fluid flow, nutrient transport and tissue growth that apply at the microscale, and present a derivation of a corresponding continuum model via a multiscale homogenisation method in §3. In §4, we present a

series of numerical experiments that indicate the model's behaviour and highlight how incorporating knowledge of tissue microstructure into such models may lead to significant differences in theoretical predictions. In §5, we summarise the main theoretical results contained within this work and their implications for tissue culture, and highlight possible future developments.

2. Theoretical formulation: a growing porous medium

We consider an idealised porous medium, represented as a highly-connected material with spatially periodic microstructure, and saturated with a viscous Newtonian fluid. Furthermore, we assume that the material can be characterised by two distinct lengthscales. The microscale domain is denoted Ω , with boundary $\partial\Omega$, and has characteristic length l^* . This is further partitioned into a fluid domain Ω_f , and a solid domain Ω_s , with boundaries $\partial\Omega_f$ and $\partial\Omega_s$, which may include parts of the exterior boundary $\partial\Omega$ and the fluid–solid interface, denoted $\partial\Omega_{fs}$. The macroscale characteristic length of the porous medium is denoted L^* , and we assume that the characteristic lengthscales are well-separated; correspondingly, we introduce a dimensionless parameter $\varepsilon > 0$ such that

$$\varepsilon = \frac{l^*}{L^*} \ll 1. \quad (2.1)$$

Throughout, asterisks distinguish dimensional quantities from their dimensionless equivalents. Figure 1 illustrates the mathematical representation of a porous material via such a periodic cell geometry.

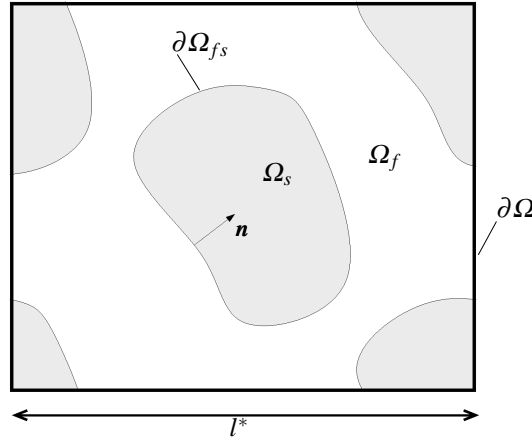


FIG. 1. Schematic diagram indicating the mathematical representation of an idealised porous material by a periodic microscale domain, Ω , of characteristic lengthscale l^* and boundary $\partial\Omega$. The periodic domain is partitioned into fluid and solid components, Ω_f (white) and Ω_s (shaded) respectively. The fluid–solid interface is denoted $\partial\Omega_{fs}$; we denote a normal to this interface (oriented pointing into the solid) by \mathbf{n} .

Flow and transport phenomena in systems of this type have been well-studied; see, for example, Mei & Auriault (1991) and, in a biological context, Shipley & Chapman (2010), and many other references therein. The key distinguishing feature of the analysis that we present is the inclusion of growth of the solid phase, coupled to flow and nutrient transport within the porous medium. This modification improves dramatically the applicability of such an idealised modelling approach to the representation of biological tissue.

The remaining assumptions underpinning our model are summarised as follows: growth of the solid domain Ω_s occurs via a change of state from fluid to solid at the interface $\partial\Omega_{fs}$, at a rate which is dependent upon the uptake from the fluid domain, Ω_f , of a generic diffusible passive nutrient. The resulting model therefore comprises an idealised description of appositional growth (in a sense that will be made clear in the following section), of broad relevance to bone tissue growth, or to the deposition of extracellular matrix (ECM) on porous scaffolds within tissue engineering bioreactors. Surface dissolution, relevant to construct dynamics post-implantation *in vivo*, may be accommodated easily within this formulation by incorporating an appropriate state change from solid to fluid.

2.1 Governing equations

The dimensional velocity of the fluid is denoted \mathbf{v}^* , with pressure p^* , and the nutrient concentration in the fluid is denoted c^* . The equations governing the fluid flow and nutrient transport at the microscale within Ω_f are as follows:

$$\rho_f^* \left(\frac{\partial \mathbf{v}^*}{\partial t^*} + (\mathbf{v}^* \cdot \nabla^*) \mathbf{v}^* \right) = -\nabla^* p^* + \mu^* \nabla^{*2} \mathbf{v}^*, \quad (2.2)$$

$$\nabla^* \cdot \mathbf{v}^* = 0, \quad (2.3)$$

$$\frac{\partial c^*}{\partial t^*} + \mathbf{v}^* \cdot \nabla^* c^* = D^* \nabla^{*2} c^*, \quad (2.4)$$

in which ρ_f^* and μ^* are the density and viscosity of the fluid, respectively, and D^* denotes the nutrient diffusivity.

As noted above, cells are not represented explicitly within our simplified formulation; instead, tissue growth associated with cell proliferation and ECM synthesis and deposition manifests itself as growth of the solid phase, which occurs via a change of state from fluid to solid, occurring at the interface $\partial\Omega_{fs}$, and dependent upon the consumption of nutrient. Enforcing mass conservation at the interface, we obtain the following boundary conditions on $\partial\Omega_{fs}$, describing nutrient consumption and the associated interfacial growth:

$$c^* (\mathbf{v}^* - \mathbf{v}_{fs}^*) \cdot \mathbf{n} - D^* \nabla^* c^* \cdot \mathbf{n} = Q^*, \quad (2.5)$$

$$\rho_f^* (\mathbf{v}^* - \mathbf{v}_{fs}^*) \cdot \mathbf{n} = -\rho_s^* \mathbf{v}_{fs}^* \cdot \mathbf{n} = S^*(Q^*), \quad (2.6)$$

in which ρ_s^* denotes the density of the solid and \mathbf{n} is the unit normal vector pointing into Ω_s . The remaining quantities \mathbf{v}_{fs}^* , the velocity of the interface, and $S^*(Q^*)$, which denotes mass conversion from fluid to solid at a rate dependent upon nutrient consumption, Q^* , are specified constitutively below.

2.1.1 Growth and nutrient uptake dynamics Equation (2.5) is a standard membrane law that describes the nutrient flux at $\partial\Omega_{fs}$, and is modified to account for interfacial movement. The mass-jump condition (2.6) is simplified by assuming that the solid phase is rigid (see Ateshian (2011) for mass-jump conditions appropriate for a growing material in a somewhat more general setting), and provides a constitutive equation defining the evolution of the fluid domain due to growth, and an explicit boundary

condition for the fluid velocity on the interface $\partial\Omega_{fs}$:

$$\mathbf{v}_{fs}^* \cdot \mathbf{n} = -\frac{1}{\rho_s^*} S^*, \quad (2.7)$$

$$\mathbf{v}^* \cdot \mathbf{n} = \left(\frac{1}{\rho_f^*} - \frac{1}{\rho_s^*} \right) S^*, \quad (2.8)$$

and so our representation of growth is of similar form to Stefan problems for phase change. We remark that due to our simplifying assumption that the solid component is rigid, momentum jump conditions across the interface are not required.

In what follows we adopt simple models for nutrient uptake and growth dynamics, and assume that nutrient uptake occurs at a rate proportional to the nutrient concentration at the interface, coupled to interfacial growth via the constitutive choices:

$$Q^* = R^* c^*, \quad S^* = \alpha^* Q^*, \quad (2.9)$$

in which the permeability, R^* , regulates the rate of nutrient consumption at the interface $\partial\Omega_{fs}$, and α^* dictates the influence of nutrient uptake upon subsequent tissue growth. To complete the system, we require that all solutions are periodic on the microscale domain Ω ; macroscale variation in Ω is of course permitted, thereby enabling spatial variation of material structure within this formulation.

We highlight that our idealised model, in which consumption and growth occur at a non-material interface ($\partial\Omega_{fs}$), may be obtained from a more complete description accounting explicitly for nutrient consumption in the tissue domain by taking the ‘thin-rim’, or ‘fast-consumption’ limit (King & Franks, 2007), in which nutrient consumption in the tissue domain dominates over diffusive transport. For clarity, denoting by c_s^* a nutrient distribution in the solid region Ω_s , with diffusivity D_s^* and consumption $\lambda^* c_s^*$, our description is appropriate in the limit $\beta = D_s^*/l^{*2}\lambda^* \ll 1$, for which nutrient consumption (and associated growth) occurs in a boundary layer of width $\mathcal{O}(\sqrt{\beta})$ with the remainder of Ω_s remaining in a necrotic or nutrient-starved state.

2.2 Nondimensionalisation

Following Shipley & Chapman (2010), we nondimensionalise as follows:

$$\mathbf{x}^* = l^* \mathbf{x}, \quad \mathbf{v}^* = V^* \mathbf{v}, \quad \mathbf{v}_{fs}^* = V^* \mathbf{v}_{fs}, \quad c^* = C^* c, \quad p^* = \frac{\mu^* L^* V^*}{l^{*2}} p, \quad t^* = \frac{L^*}{V^*} t, \quad (2.10)$$

in which V^* and C^* are characteristic macroscale flow velocity and nutrient concentration scales. Therefore, the timescale under consideration is that of macroscale advection. We remark that the timescale of microscale growth could be analysed via the choice $t^* = l^* t/V_m^*$ (where V_m^* is an appropriate microscale velocity scale); however, such a scaling increases the complexity of the governing equations that result and is therefore not considered here. We note also that the Poiseuille-type pressure scaling is key to obtaining the proper leading-order problem in the models that we develop below.

In dimensionless form, the equations governing flow and transport in Ω_f are:

$$\varepsilon^2 \text{Re} \left(\varepsilon \frac{\partial \mathbf{v}}{\partial t} + (\mathbf{v} \cdot \nabla) \mathbf{v} \right) = -\nabla p + \varepsilon \nabla^2 \mathbf{v}, \quad (2.11)$$

$$\nabla \cdot \mathbf{v} = 0, \quad (2.12)$$

$$\varepsilon \frac{\partial c}{\partial t} + \mathbf{v} \cdot \nabla c = \frac{1}{\text{Pe}} \nabla^2 c; \quad (2.13)$$

and the boundary conditions on the interface $\partial\Omega_{fs}$ read:

$$c(\mathbf{v} - \mathbf{v}_{fs}) \cdot \mathbf{n} - \frac{1}{\text{Pe}} \nabla c \cdot \mathbf{n} = Q, \quad (2.14)$$

$$\mathbf{v} \cdot \mathbf{n} = (\rho - 1)S. \quad (2.15)$$

The velocity of the solid–fluid interface in the normal direction, and the dimensionless interfacial growth S and nutrient consumption Q are given by

$$\mathbf{v}_{fs} \cdot \mathbf{n} = -S, \quad Q = Rc, \quad S = \alpha Q. \quad (2.16)$$

The Reynolds number and Péclet number, appropriate for macroscale advective flow are defined by:

$$\text{Re} = \frac{\rho_f^* V^* L^*}{\mu^*}, \quad \text{Pe} = \frac{V^* l^*}{D^*}, \quad (2.17)$$

and the remaining dimensionless groupings appearing in (2.11)–(2.16) are: $\rho = \rho_s^*/\rho_f^*$, the relative density; $R = R^*/V^*$, a parameter controlling the rate of nutrient consumption by the solid phase at the fluid–solid interface; and $\alpha = \alpha^* C^*/\rho_s^*$, which controls the rate of growth that results from nutrient consumption.

Together with the requirement that the solutions be periodic on Ω (macroscale variations are admitted), Equations (2.11)–(2.16), comprise the microscale ‘cell problem’, describing the growing porous medium. In what follows, we employ this microscale model to obtain a macroscale representation of flow and transport phenomena within a growing porous medium, under simple assumptions of growth and consumption dynamics. The cell problem that we consider is chosen to be particularly simple, the better to highlight how growth may be accommodated within such a formulation.

3. Multiple scales analysis

We now analyse (2.11)–(2.14) via a multiple-scales method, with the aim of deriving a macroscale description which incorporates the microscale growth defined in (2.16). We reiterate that we follow closely the method outlined in Burridge & Keller (1981), Shipley & Chapman (2010) and many others; the key distinguishing feature of this analysis is the inclusion of growth of the solid phase in response to nutrient consumption.

We introduce a dimensionless macroscale coordinate \mathbf{X} , related to the microscale variable \mathbf{x} via $\mathbf{x} = \varepsilon^{-1}\mathbf{X}$; under the assumption of scale separation, we expand all dependent variables ψ in multiple-scales form:

$$\psi(\mathbf{x}, \mathbf{X}, t; \varepsilon) = \psi^{(0)}(\mathbf{x}, \mathbf{X}, t) + \varepsilon \psi^{(1)}(\mathbf{x}, \mathbf{X}, t) + \dots, \quad (3.1)$$

and note that under this coordinate transformation,

$$\nabla = \nabla_{\mathbf{x}} + \varepsilon \nabla_{\mathbf{X}}, \quad \nabla^2 = \nabla_{\mathbf{x}}^2 + 2\varepsilon \nabla_{\mathbf{x}} \cdot \nabla_{\mathbf{X}} + \varepsilon^2 \nabla_{\mathbf{X}}^2, \quad (3.2)$$

where $\nabla_{\mathbf{x}}$, $\nabla_{\mathbf{X}}$, $\nabla_{\mathbf{x}}^2$ and $\nabla_{\mathbf{X}}^2$ denote the gradient and Laplacian operators in the micro- and macroscale descriptions.

Our aim is to employ the representation (3.1), (3.2) to obtain a description of the flow, nutrient transport and tissue growth at the macroscale, obtained from the microscale dynamics. Of use will be the following integral average defined, for some quantity g :

$$\langle g \rangle_f = \frac{1}{|\Omega_f|} \int_{\Omega_f} g \, dV. \quad (3.3)$$

Additionally, we denote the porosity of the material by $\Phi_f = |\Omega_f|/|\Omega|$; the pore surface area is defined by $|\partial\Omega_{fs}|$. Important to the method that we employ is the conversion, via the divergence theorem, of volume integrals of the form (3.3) to those over the pore surface. Correspondingly, we introduce the following notation:

$$\langle g \rangle_{fs} = \frac{1}{|\Omega|} \int_{\partial\Omega_{fs}} g \, dS. \quad (3.4)$$

3.1 Microscale flow and transport

At $\mathcal{O}(1)$, the governing equations and boundary conditions reduce to:

$$\nabla_x p^{(0)} = \mathbf{0}, \quad \nabla_x \cdot \mathbf{v}^{(0)} = 0, \quad \mathbf{x} \in \Omega_f, \quad (3.5)$$

$$\frac{1}{\text{Pe}} \nabla_x^2 c^{(0)} - \mathbf{v}^{(0)} \cdot \nabla_x c^{(0)} = 0, \quad \mathbf{x} \in \Omega_f \quad (3.6)$$

$$\mathbf{v}^{(0)} \cdot \mathbf{n} = (\rho - 1)S^{(0)}, \quad \mathbf{x} \in \partial\Omega_{fs}, \quad (3.7)$$

$$c^{(0)} \left(\mathbf{v}^{(0)} - \mathbf{v}_{fs}^{(0)} \right) \cdot \mathbf{n} - \frac{1}{\text{Pe}} \nabla_x c^{(0)} \cdot \mathbf{n} = Q^{(0)}, \quad \mathbf{x} \in \partial\Omega_{fs}, \quad (3.8)$$

$$\mathbf{v}_{fs}^{(0)} \cdot \mathbf{n} = -S^{(0)}, \quad \mathbf{x} \in \partial\Omega_{fs}, \quad (3.9)$$

together with the requirement that solutions be periodic on Ω . We highlight that, for the sake of generality, we do not replace the interfacial transport terms S and Q by (2.16) in the following derivation.

The first of Equations (3.5) indicates that $p^{(0)} = p^{(0)}(\mathbf{X}, t)$, so that the pressure is constant on the microscale. This implies that the microscale growth embodied by (3.7) and (3.9) cannot lead to a corresponding microscale pressure-induced flow. For consistency, we therefore relegate interfacial growth (and associated nutrient uptake) to $\mathcal{O}(\varepsilon)$; the necessity of such a rescaling is a consequence of (2.10), in which we choose a Poiseuille scaling for the pressure, and analyse processes on the timescale of macroscale advection. Alternative choices (such as a microscale growth timescale) permit leading order microscale growth but increase significantly the complexity of the flow equations, by introducing inertial terms associated with leading-order variations in the microscale geometry, for example.

In view of the above, in what follows we employ the rescaling $R = \varepsilon \hat{R}$ (but omit carets for brevity), so that

$$S^{(0)} = 0, \quad Q^{(0)} = 0. \quad (3.10)$$

We adopt this scaling, for which changes in the geometry of Ω associated with growth appear at $\mathcal{O}(\varepsilon)$, to reflect the case for which the leading order unit cell problem is particularly simple. However, below, we will show that despite its relegation to lower order, the evolution of the microscale geometry under the influence of interfacial microscale growth is, nevertheless, evident in the leading order macroscale fluid flow and nutrient transport. We note in passing that Shipley & Chapman (2010) motivate similar choices by detailed consideration of experimental results obtained in the context of drug delivery to tumours.

On application of the rescalings, the leading order problem reduces to $p^{(0)} = p^{(0)}(\mathbf{X}, t)$, $\mathbf{v}_{fs}^{(0)} = \mathbf{0}$. In addition, multiplying (3.6) by $c^{(0)}$, integrating over Ω_f , and employing the divergence theorem together with the boundary conditions (3.7) and (3.8) (which now amount to no-penetration and no-flux conditions) and microscale periodicity, reveals that the nutrient concentration is locally constant: $c^{(0)} = c^{(0)}(\mathbf{X}, t)$.

In summary, the leading order problem is $p^{(0)} = p^{(0)}(\mathbf{X}, t)$, $\mathbf{v}_{fs}^{(0)} = \mathbf{0}$, $c^{(0)} = c^{(0)}(\mathbf{X}, t)$ and:

$$\nabla_{\mathbf{x}} \cdot \mathbf{v}^{(0)} = 0, \quad \mathbf{x} \in \Omega_f \quad (3.11)$$

$$\mathbf{v}^{(0)} \cdot \mathbf{n} = 0, \quad \mathbf{x} \in \partial\Omega_{fs}, \quad (3.12)$$

and so the leading order microscale problem is under-determined for flows in more than one spatial dimension.

At $\mathcal{O}(\varepsilon)$, the equations read:

$$\mathbf{0} = -\nabla_{\mathbf{x}} p^{(1)} - \nabla_{\mathbf{X}} p^{(0)} + \nabla_{\mathbf{x}}^2 \mathbf{v}^{(0)}, \quad \mathbf{x} \in \Omega_f \quad (3.13)$$

$$0 = \nabla_{\mathbf{x}} \cdot \mathbf{v}^{(1)} + \nabla_{\mathbf{X}} \cdot \mathbf{v}^{(0)}, \quad \mathbf{x} \in \Omega_f \quad (3.14)$$

$$\frac{\partial c^{(0)}}{\partial t} + \mathbf{v}^{(0)} \cdot (\nabla_{\mathbf{X}} c^{(0)} + \nabla_{\mathbf{x}} c^{(1)}) = \frac{1}{\text{Pe}} \nabla_{\mathbf{x}}^2 c^{(1)}, \quad \mathbf{x} \in \Omega_f \quad (3.15)$$

$$\mathbf{v}^{(1)} \cdot \mathbf{n} = (\rho - 1)S^{(1)}, \quad \mathbf{x} \in \partial\Omega_{fs}, \quad (3.16)$$

$$\frac{1}{\text{Pe}} \nabla_{\mathbf{x}} c^{(1)} \cdot \mathbf{n} = c^{(0)} (\mathbf{v}^{(1)} - \mathbf{v}_{fs}^{(1)}) \cdot \mathbf{n} - \frac{1}{\text{Pe}} \nabla_{\mathbf{X}} c^{(0)} \cdot \mathbf{n} - Q^{(1)}, \quad \mathbf{x} \in \partial\Omega_{fs}, \quad (3.17)$$

$$\mathbf{v}_{fs}^{(1)} \cdot \mathbf{n} = -S^{(1)}, \quad \mathbf{x} \in \partial\Omega_{fs}, \quad (3.18)$$

where the microscale invariance of $p^{(0)}$ and $c^{(0)}$, and the leading order boundary conditions, have been employed to simplify the equations. In the current application, we anticipate that the density of the growing porous medium will exceed that of the culture medium so that $\rho > 1$; therefore, (3.16) shows that growth of the solid phase leads naturally to fluid flow towards the interface $\partial\Omega_{fs}$ ($\mathbf{v}^{(1)} \cdot \mathbf{n} > 0$) in order to conserve mass.

An appropriate form for the microscale leading order flow may be obtained by exploiting the linearity of Equations (3.11) and (3.13), and the independence of $p^{(0)}$ on the microstructure:

$$\mathbf{v}^{(0)} = -\mathbf{K} \nabla_{\mathbf{X}} p^{(0)}, \quad (3.19)$$

$$p^{(1)} = -\mathbf{a} \cdot \nabla_{\mathbf{X}} p^{(0)} + \bar{p}_1, \quad (3.20)$$

in which $\bar{p}_1 = \bar{p}_1(\mathbf{X}, t)$, while the permeability tensor \mathbf{K} and the vector \mathbf{a} , which imparts microscale variation to the $\mathcal{O}(\varepsilon)$ pressure, exhibit both micro- and macroscale dependence, but are independent of time at leading order (as a consequence of the quasi-static domain Ω). We obtain the following Stokes flow boundary value problem on the periodic cell:

$$\nabla_{\mathbf{x}} \cdot \mathbf{K} = 0, \quad \mathbf{x} \in \Omega_f, \quad (3.21)$$

$$-\nabla_{\mathbf{x}} \mathbf{a} + \nabla_{\mathbf{x}}^2 \mathbf{K} = -\mathbf{I}, \quad \mathbf{x} \in \Omega_f, \quad (3.22)$$

$$\mathbf{K} = \mathbf{0}, \quad \mathbf{x} \in \partial\Omega_{fs}, \quad (3.23)$$

and \mathbf{K} and \mathbf{a} periodic on Ω . Equations (3.21)–(3.23) do not specify uniquely the microscale variable \mathbf{a} ; therefore, we impose the additional integral constraint:

$$\langle \mathbf{a} \rangle_f = \mathbf{0}. \quad (3.24)$$

The cell problem given by Equations (3.21)–(3.24) may, in principle, be solved for any given choice of Ω , which reflects the microscale geometry of the porous material. In general, this problem requires

numerical solution (see Zick & Homsy (1982) and earlier references therein); however, analytic results are possible in some simplified geometries – see, *e.g.*, Shipley (2008) for example calculations.

The corresponding nutrient transport is governed by (3.15), subject to (3.17) and (3.18), which is insufficient to determine $c^{(0)}$. However, our focus in this paper is the generation of appropriate *macroscale* models, suitable to describe flow, transport and growth; in what follows we show how the above (well-known) microscale Stokes formulation, together with the $\mathcal{O}(\varepsilon)$ system (3.13)–(3.18) may be exploited to determine flow and nutrient transport at the macroscale in the presence of microscale nutrient-limited growth.

3.2 Macroscale flow and transport

To obtain the macroscale flow and nutrient transport equations, we exploit the integral average (3.3). The macroscale leading-order flow description is obtained by averaging Equation (3.19) to obtain

$$\langle \mathbf{v}^{(0)} \rangle_f = -\langle \mathbf{K} \rangle_f \cdot \nabla_X p^{(0)}, \quad (3.25)$$

which is the well-known Darcy description of flow through a porous medium.

An equation governing the leading-order macroscale pressure is obtained in the following way. Averaging (3.14) over the periodic cell and exploiting (3.4) supplies:

$$\nabla_X \cdot \langle \mathbf{v}^{(0)} \rangle_f = (1 - \rho) \langle S^{(1)} \rangle_{fs}, \quad (3.26)$$

in which the divergence theorem has been employed to transform the volume integral over Ω_f to one over the surface $\partial\Omega_f$, which comprises, in general, both the interfacial surface $\partial\Omega_{fs}$ and parts of the exterior boundary, $\partial\Omega$. The boundary condition (3.16) is exploited to express the normal flow velocity in terms of the microscale growth, and periodicity of solutions over Ω implies that contributions arising from exterior surfaces cancel out, leaving those from the interfacial surface $\partial\Omega_{fs}$ only. Combining (3.25) and (3.26) then yields

$$\nabla_X \cdot \left(\langle \mathbf{K} \rangle_f \nabla_X p^{(0)} \right) = (\rho - 1) \langle S^{(1)} \rangle_{fs}. \quad (3.27)$$

We remark that the quasi-static microscale pore geometry Ω defines the flow characteristics via the averaged porosity tensor $\langle \mathbf{K} \rangle_f$, which contains information from the underlying microstructure, and may additionally vary on the macroscale. Furthermore, although microscale growth enters the problem at $\mathcal{O}(\varepsilon)$, it influences nevertheless the leading-order flow via contributions to the macroscale pressure in (3.27).

In the current work, growth is coupled explicitly to the leading-order nutrient consumption at the interface via (2.16) (and (3.10)). Although the nutrient transport problem given by (3.15) and (3.17) is insufficient to determine the microscale nutrient transport and consumption dynamics, below, we show that leading-order macroscale description suitable to specify fully the macroscale flow, transport and growth dynamics may be obtained.

Integrating (3.15) over Ω_f , and applying the divergence theorem and the leading order no-penetration condition (3.12), yields:

$$\Phi_f \frac{\partial c^{(0)}}{\partial t} + \langle \mathbf{v}^{(0)} \rangle_f \cdot \nabla_X c^{(0)} = \frac{1}{\text{Pe}} \langle \nabla_X c^{(1)} \cdot \mathbf{n} \rangle_{fs}, \quad (3.28)$$

wherein Φ_f denotes the porosity of the material, and as previously, we note that contributions associated with changes in the integration domain are relegated to lower order.

The $\mathcal{O}(\varepsilon)$ diffusive nutrient flux over the solid–fluid interface in (3.28) may be obtained in terms of the leading-order macroscale concentration by integrating (3.17) over the interface $\partial\Omega_{fs}$, and applying the leading order no-penetration and no-concentration flux conditions, together with the $\mathcal{O}(\varepsilon)$ microscale interfacial growth conditions (3.16) and (3.18). After some algebra, the following advection–reaction equation governing macroscale nutrient transport is obtained:

$$\Phi_f \frac{\partial c^{(0)}}{\partial t} + \langle \mathbf{v}^{(0)} \rangle_f \cdot \nabla_X c^{(0)} = \rho c^{(0)} \langle S^{(1)} \rangle_{fs} - \langle Q^{(1)} \rangle_{fs}, \quad (3.29)$$

in which the interfacial growth and nutrient consumption terms are defined by (2.16), (3.10) as:

$$Q^{(1)} = Rc^{(0)}, \quad S^{(1)} = \alpha Q^{(1)}. \quad (3.30)$$

We remark that interfacial growth appears as an apparent source in Ω_f because, for certain choices of α and ρ , the fluid being used to create the (denser) solid material at $\partial\Omega_{fs}$ contains more nutrient than is required; in fact, the model requires $0 \leq \alpha\rho \leq 1$ in order that the dimensionless nutrient concentration does not exceed $c = 1$. Such behaviour arises due to our simplified ‘thin-rim’ model representation, in which growth is described by a Stefan-type phase change process. A more complete description would, presumably, prohibit this; we therefore expect that it will not be observed for physiologically-relevant choices of α and ρ .

In summary, our macroscale representation of microscale surface accretion in a porous material comprises the flow problem governed by Equations (3.25) and (3.27), coupled to the nutrient transport problem given by Equation (3.29), via the nutrient consumption-dependent growth (3.30). These equations are subject to suitable initial and boundary data on the macroscale, to be defined below. The dependence of the flow and transport dynamics on the porous microstructure is provided by the permeability tensor \mathbf{K} , obtained from (3.21)–(3.24). We remark that our model formulation is similar in form to that derived in Shipley & Chapman (2010), which considered drug transport from a fluid to a porous medium (see Equations (70), (75), (126), (127) of that paper) in the context of tumour therapy; however, in this work, contributions to the fluid pressure, and effective source/sink terms in the nutrient concentration equations arise due to tissue growth. We highlight that although the preceding analysis considers microscale growth which is slow in comparison to the macroscale advection-based timescale (and therefore appears at $\mathcal{O}(\varepsilon)$) it is evident in the leading order macroscale problem that we derive.

4. Numerical results

We now present a series of illustrative numerical simulations of equations (3.21)–(3.24), and (3.25), (3.27), (3.29) and (3.30) chosen (i) to highlight how microscale growth and uptake influence transport in an idealised porous medium; (ii) to indicate how microstructural information may be easily integrated within such a model; and (iii) to demonstrate how its inclusion influences significantly the predicted flow and transport dynamics in structures of relevance to tissue engineering applications.

To achieve this, in §4.1, we consider the case for which the choice of the microscale domain Ω is inspired by μ CT (micro computed tomography) data obtained from a typical tissue engineering scaffold, and provide illustrative numerical solutions indicating the influence of such a geometry on the microscale dynamics. In §4.2 we employ this information within the macroscale equations, and compare the resulting numerical predictions with those that arise when such a microstructure is replaced by an array of circular obstructions; the substantial influence of our new macroscale formulation on model dynamics, in comparison to standard representations of porous flow, is highlighted by contrasting the results obtained in the presence and absence of growth.

4.1 Microscale geometry

In this subsection, we consider a specific microscale geometry inspired by *in vitro* tissue engineering applications, with which to define our domain Ω ; for simplicity, we restrict attention to flow, nutrient transport and growth in two dimensions.

A typical method to create tissue constructs of a size suitable for implantation (while minimising the necrotic core that often forms at the centre of such constructs) is to employ advection of culture medium within a perfusion bioreactor to enhance oxygen/nutrient delivery to cells. Such an approach is used by El Haj and coworkers within a bioreactor system that comprises a cell-seeded poly(L-lactic acid) (PLLA) scaffold (depicted in Figure 2(a)), through which culture medium is perfused (El Haj *et al.*, 1990; Baas *et al.*, 2010). We employ data obtained from μ CT scans of such a PLLA scaffold to define our periodic microscale domain Ω ; in this context, the microscale growth embodied by (3.30) represents ECM deposition and/or mineralisation on the pore surface by a cell population seeded within the scaffold.

Figure 2(b) indicates a typical two-dimensional section of the scaffold, together with our chosen computational domain. The porosity of such a scaffold is $\Phi_f = 0.9$ (Baas *et al.*, 2010) and we choose the relative areas of Ω_f and Ω_s in our computational domain to reflect this. When such a scaffold is seeded with human bone cells and cultured for four weeks, deposition of extracellular materials and subsequent mineralisation reduce the porosity by approximately 2% to $\Phi_f \approx 0.88$ (data omitted; see Baas *et al.* (2010) for details). Such a deposition and mineralisation rate provides additional justification for our earlier assumption that the rate of interfacial growth may be specified as $S = \mathcal{O}(\varepsilon)$.

We remark that the PLLA scaffold illustrated in Figure 2 exhibits a highly inter-connected microstructure, with a significant degree of randomness: repeating periodically our computational unit Ω does not represent accurately such scaffold. We note, furthermore, that since we restrict attention to two spatial dimensions for simplicity, the connected three-dimensional skeleton depicted in Figure 2(a) appears as an array of disconnected masses. We reiterate, however, that in choosing this geometry for Ω our aim is not to represent comprehensively the processes of tissue growth within a specific *in vitro* system, but to illustrate the ease with which suitable experimental data may be incorporated and, together with microscale growth, to highlight its importance in model dynamics.

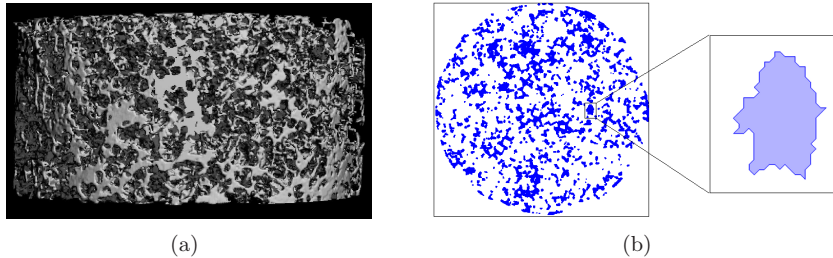


FIG. 2. (a) μ CT (micro computed tomography) image of a typical PLLA scaffold employed in a perfusion tissue culture system (Baas *et al.*, 2010). Dimensions are: 9 mm (diameter), 4 mm (height). (b) A two-dimensional section of the scaffold shown in (a). Blue regions indicate solid matrix (colour online). Inset: a typical element of the scaffold microstructure, which we employ as our chosen representative microscale domain in Section 4

Numerical solutions of the microscale problem given by Equations (3.21)–(3.24) in the computational domain illustrated in Figure 2(b) were obtained via a finite element method, implemented in the software COMSOL Multiphysics. These results are illustrated in Figure 3 and indicate clearly the strong

microscale variation in the local permeability tensor \mathbf{K} , and the microscale $\mathcal{O}(\varepsilon)$ pressure contribution \mathbf{a} . Figures 3(a–d) highlight additionally the disparity in permeability in different coordinate directions, indicating that anisotropy in the porous material’s flow properties is induced by the microstructure.

4.2 Macroscale dynamics

In this subsection, we indicate how the microscale results depicted in Figure 3 determine the macroscale flow, nutrient transport and growth characteristics via Equations (3.25), (3.27), (3.29) and (3.30), subject to suitable boundary and initial conditions to be specified below. To highlight its importance, we contrast these results with those obtained when the complex geometry indicated in Figure 2 is replaced by a set of circular obstructions, also obeying $\Phi_f = 0.9$.

The influence of the underlying porous microstructure is evident in the macroscale dynamics via the average permeability, $\langle \mathbf{K} \rangle_f$, calculated from the solutions to (3.21)–(3.24) via numerical quadrature. Employing the results illustrated in Figure 3, and corresponding solutions obtained in the case for which Ω_s is a circle, we obtain the following macroscale permeability tensors:

$$\langle \mathbf{K}^{\mu CT} \rangle_f = \begin{pmatrix} 0.37 & 0.0014 \\ 0.0014 & 0.64 \end{pmatrix}, \quad \langle \mathbf{K}^\bullet \rangle_f = \begin{pmatrix} 1.46 & 0 \\ 0 & 1.46 \end{pmatrix}, \quad (4.1)$$

in which the superscripts ‘ μCT ’ and ‘ \bullet ’ differentiate the permeability tensors associated with each microscale geometry. Comparison of the permeability in each case highlights the degree of macroscale anisotropy imparted by the porous microgeometry; the absence of macroscale variation in $\langle \mathbf{K} \rangle_f$ is a consequence of the periodic material under consideration. For brevity, solutions equivalent to those shown in Figure 3 for the case of a circular obstruction are not included here – a corresponding calculation is provided in Zick & Homsy (1982).

To define our macroscale initial and boundary conditions and computational domain, we consider an idealised model of the perfusion bioreactor described above, represented by the two-dimensional region $-0.5 \leq X \leq 0.5$, $-1 \leq Y \leq 1$, and subject to an imposed axial pressure drop, which drives a flow of culture medium. We investigate how the transport of a diffusible nutrient through the system is influenced by the nutrient-dependent microscale growth of the solid component. Appropriate boundary conditions on $p^{(0)}$, $c^{(0)}$ are as follows:

$$p^{(0)} = P_0, \quad c^{(0)} = C_0, \quad Y = 1, \quad (4.2)$$

$$p^{(0)} = 0, \quad Y = -1, \quad (4.3)$$

$$\langle \mathbf{K}^i \rangle_f \nabla_X p^{(0)} \cdot \mathbf{n} = 0, \quad \frac{\partial c^{(0)}}{\partial X} = 0, \quad X = \pm 0.5, \quad (4.4)$$

where $i \in \{\mu CT, \bullet\}$ denotes each microstructure. These boundary conditions represent a line source of nutrient introduced at $Y = 1$, which is transported through the porous medium via a pressure-driven flow of culture medium, with no-penetration of culture medium or nutrient through the bioreactor walls. The averaged culture medium velocity $\langle \mathbf{v}^{(0)} \rangle_f$ is calculated from $p^{(0)}$ via (3.25) and (4.1). We are interested in the transport of nutrient through the scaffold, and its uptake by the solid phase, leading to tissue growth; we therefore specify the following initial data: $c^{(0)}(\mathbf{X}, 0) = 0$.

In addition to the imposed pressure drop, P_0 , and nutrient source, C_0 , the macroscale problem contains the following dimensionless parameters: R , α and ρ which determine the rate of nutrient consumption by the interface, its influence on growth and the relative density of the fluid and solid phases (the

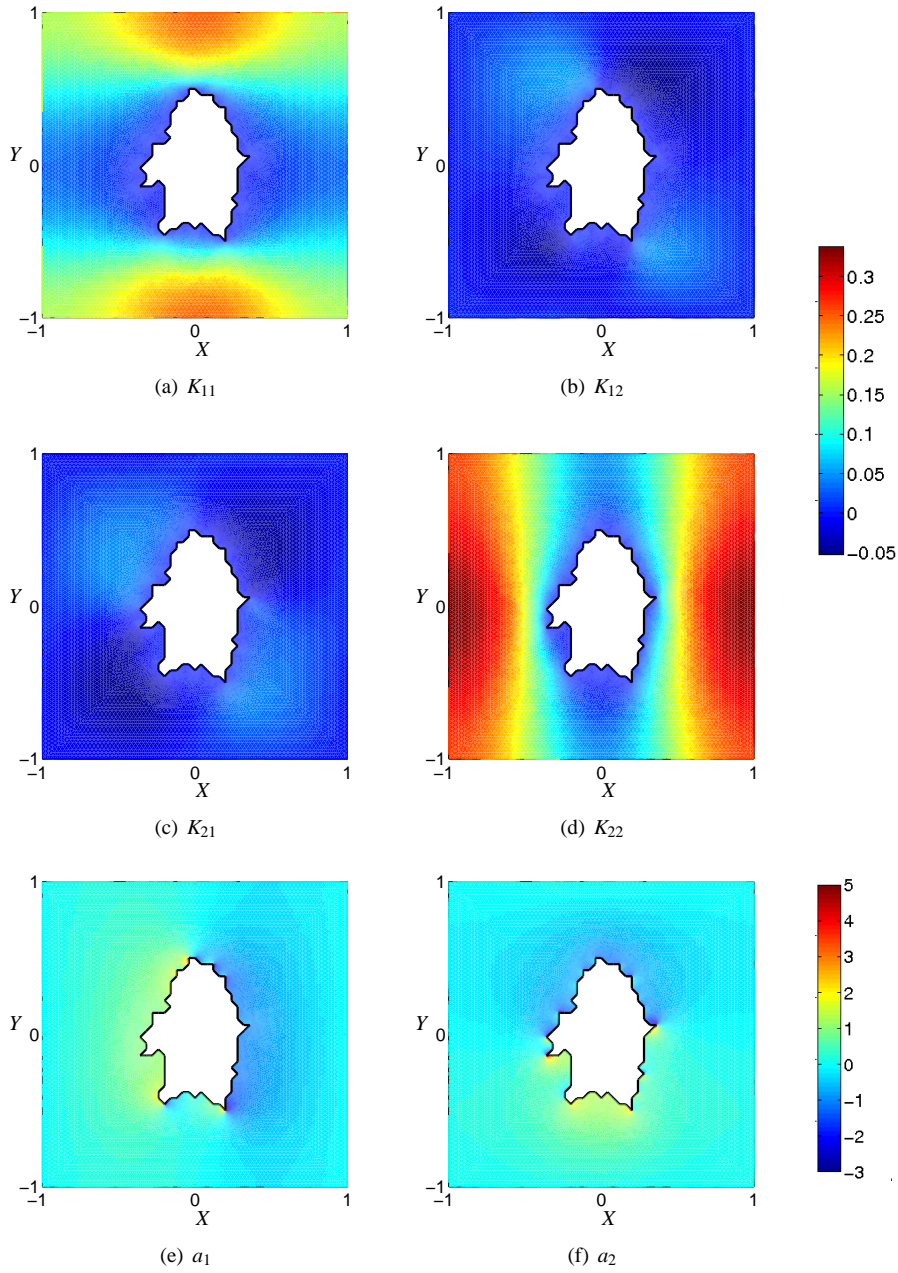


FIG. 3. Numerical solutions of the microscale Stokes problem (3.21)–(3.24) in the computational domain defined in Figure 2 with $\Phi_f = 0.9$, illustrating how microscale variation is imparted to the flow via (3.19) and (3.20) due to the microstructure. (a)–(d) the components of the permeability tensor, \mathbf{K} ; (e), (f) the components of the $\mathcal{O}(\varepsilon)$ pressure contribution, \mathbf{a} .

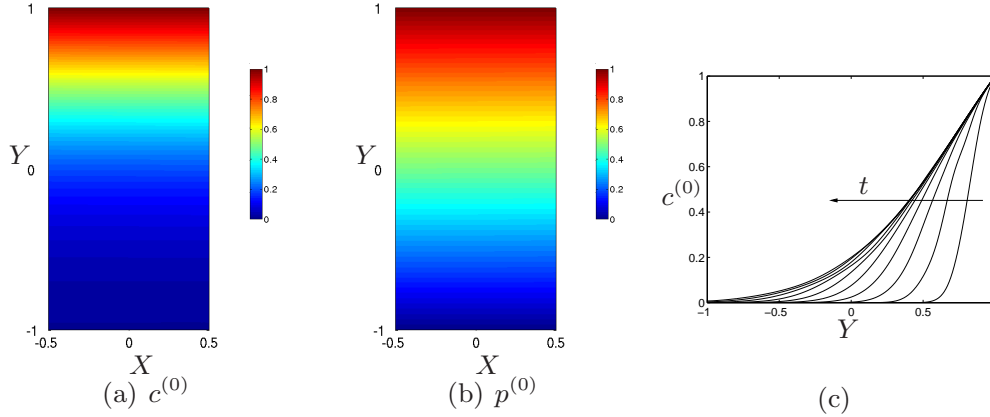


FIG. 4. Numerical solutions of the macroscale model (3.25), (3.27), (3.29)–(4.4), indicating (a) the macroscale nutrient distribution $c^{(0)}$, and (b) pressure field $p^{(0)}$ within a PLLA scaffold (with the periodic microstructure illustrated in Figure 2) at $t = 10$ (dimensionless units), by which time the system has relaxed to a steady state. (c) The nutrient distribution at $X = 0$ at $t = 0, 1, 2, \dots, 10$, indicating convergence to an axially nonuniform steady state (the arrow indicates the direction of increasing t). Parameter values: $P_0 = C_0 = R = 1$, $\alpha = 0.5$, $\rho = 1.25$, $\Phi_f = 0.9$.

remaining constants that appear in the equations arise via (3.4), and are fixed by the geometry of Ω . In the context of a mineralised rim of similar density to the underlying PLLA scaffold being deposited upon the pore surface, an appropriate choice for relative density is in the range $\rho = 1.25$ – 1.29 (Mikos *et al.*, 1994), and for the reasons discussed above, we require $\alpha \leq 1/\rho$. We emphasise that our focus here is on highlighting model dynamics for a particular porous structure; therefore, we choose not to consider specific uptake/consumption parameters appropriate for individual tissue engineering applications, and nor do we undertake a detailed parameter study. In the numerical simulations that follow, we fix $P_0 = C_0 = 1$, and indicate the behaviour of the model for representative values of the parameters relating to uptake and growth (detailed in the relevant figure captions).

Figures 4(a,b) show typical numerical results, at a representative time point ($t = 10$), indicating the distribution of nutrient and fluid pressure field on the macroscale, within a porous scaffold with microstructure illustrated in Figure 2(b) (that is, the permeability tensor is $\langle \mathbf{K}^{\mu\text{CT}} \rangle_f$). These highlight that nutrient spreads through the porous scaffold under the influence of the pressure-induced flow, but that the extent of nutrient advection is limited. Figure 4(c) shows the time evolution of the nutrient concentration at $X = 0$, indicating clearly that transport of nutrient from upstream regions slows, eventually achieving a steady configuration in which regions distant from the source exhibit nutrient depletion so that, due to (3.30), uptake and associated growth is restricted to upstream regions. We remark that these ‘steady-state’ solutions have not been verified analytically; however, our numerical experiments indicate that these represent configurations whose time-evolution is minimal. Below, we will employ the terminology ‘steady-state’, for concision.

We highlight that due to the problem set-up, and the representation of culture medium flow by a Darcy law (which prohibits application of no-slip on the bioreactor walls), the solutions shown in Figures 4(a,b) display very little dependence on the transverse coordinate.

In Figures 5 and 6 these results are analysed in more detail. In Figures 5(a,c,e), we present the nutrient concentration, fluid pressure and axial velocity at $X = 0$ ($t = 10$), while Figures 5(b,d,f) indicate how the nutrient transport is influenced by changes in ρ , α and R . To highlight the influence of

the microscale scaffold anisotropy on our model predictions, in Figures 5(a,c,e) we include simulation results obtained in the case for which the periodic microstructure comprises an array of circles; *i.e.* the permeability is $\langle \mathbf{K}^\bullet \rangle_f$. The specific influence of microscale growth is indicated in Figure 6, in which the predicted flow and transport characteristics in its presence and absence are contrasted.

Our results indicate clearly that significant axial variation in flow and transport characteristics is induced by the PLLA scaffold's porous structure, and its microscale growth. Figures 5(a,c,e) show that in such a structure, nutrient uptake is increased dramatically, leading to reduced flow and downstream nutrient starvation; reduced growth associated with such nutrient depletion leads to axially-varying flow and pressure profiles via (3.27). In contrast, when Ω_s is circular, dramatically enhanced flow and transport are observed. The stark differences in flow and transport highlighted by Figures 5(a,c) arise from the microstructure of the porous material. Nutrient consumption and subsequent growth depend on the size of the solid–fluid interface $\partial\Omega_{fs}$; see (3.4), (3.29) and (3.30). The irregular nature of the obstructions in our representation of the PLLA scaffold leads to an (approx.) 3-fold increase in interfacial size (data omitted), when compared to an array of circular obstructions. Therefore, nutrient provided by the source at $Y = 1$ is consumed by the solid phase more rapidly in such a structure, leading to significant axial variation in growth and flow.

Figures 5(b,d,f) indicate that the axially-dependent steady states discussed arise via a balance being established between advective transport and consumption of nutrient by the growing rim, governed by the parameters R , α , ρ . Figure 5(b) shows that increased consumption by the growing rim leads to a significant reduction in nutrient transport through the domain, leading to growth being localised by the nutrient source at $Y = 1$, only. Figures 5(d,f) show how the density of the growing solid, and the ‘efficiency’ with which it is created (via ρ and α , respectively) influences nutrient transport. As highlighted previously, growth manifests itself as an apparent source of nutrient in Ω_f , reflecting the possibility that the fluid contains unrequired nutrient; as the fluid is converted, this nutrient is left behind. Figures 5(d,f) highlight that the creation of dense material (which requires a larger volume of fluid), or highly efficient growth (requiring little nutrient), leads to a significant nutrient source, aiding transport through the scaffold. As discussed in §3.2, such behaviour is an interesting facet of the model, but it is anticipated that physiologically-relevant choices of α and ρ would prohibit this.

The influence of microscale growth on the macroscale predictions is highlighted explicitly in Figure 6. In the absence of growth and associated uptake ($R = 0$), (3.27), (4.1) and (4.4) provide $p^{(0)} = (Y + 1)/2$ so that the leading-order macroscale velocity in each geometry is constant and given by:

$$\langle \mathbf{v}^{(0)} \rangle_f^{\mu CT} = (-0.0007, -0.32), \quad \langle \mathbf{v}^{(0)} \rangle_f^\bullet = (0, -0.73), \quad (4.5)$$

where, as in (4.1), the superscripts indicate the microscale geometry. Figure 6(a) indicates the disparity between such constant flow solutions and those obtained in the presence of growth, highlighting that tissue growth leads to flow restriction and axial variations in flow speed. The results in Figure 6(b) demonstrate that in the absence of growth and associated uptake, nutrient transport is complete in contrast to the steady-state nutrient distributions obtained in Figures 4 and 5, which arise from a balance between uptake associated with growth, and advective transport.

We note that in such a parameter regime (and for suitable initial data) nutrient transport takes the form of a plane travelling wave, and we may construct explicit analytical solutions of the form:

$$c^{(0)} = g(\mathbf{X} - \langle \mathbf{v}^{(0)} \rangle_f t), \quad (4.6)$$

where $g = c^{(0)}(\mathbf{X}, 0)$ denotes the initial nutrient profile ($c^{(0)} = 1$ at $Y = 1$, $c^{(0)} = 0$ elsewhere), and the macroscale advective flow velocity is given for each microstructure in (4.5). This solution describes a

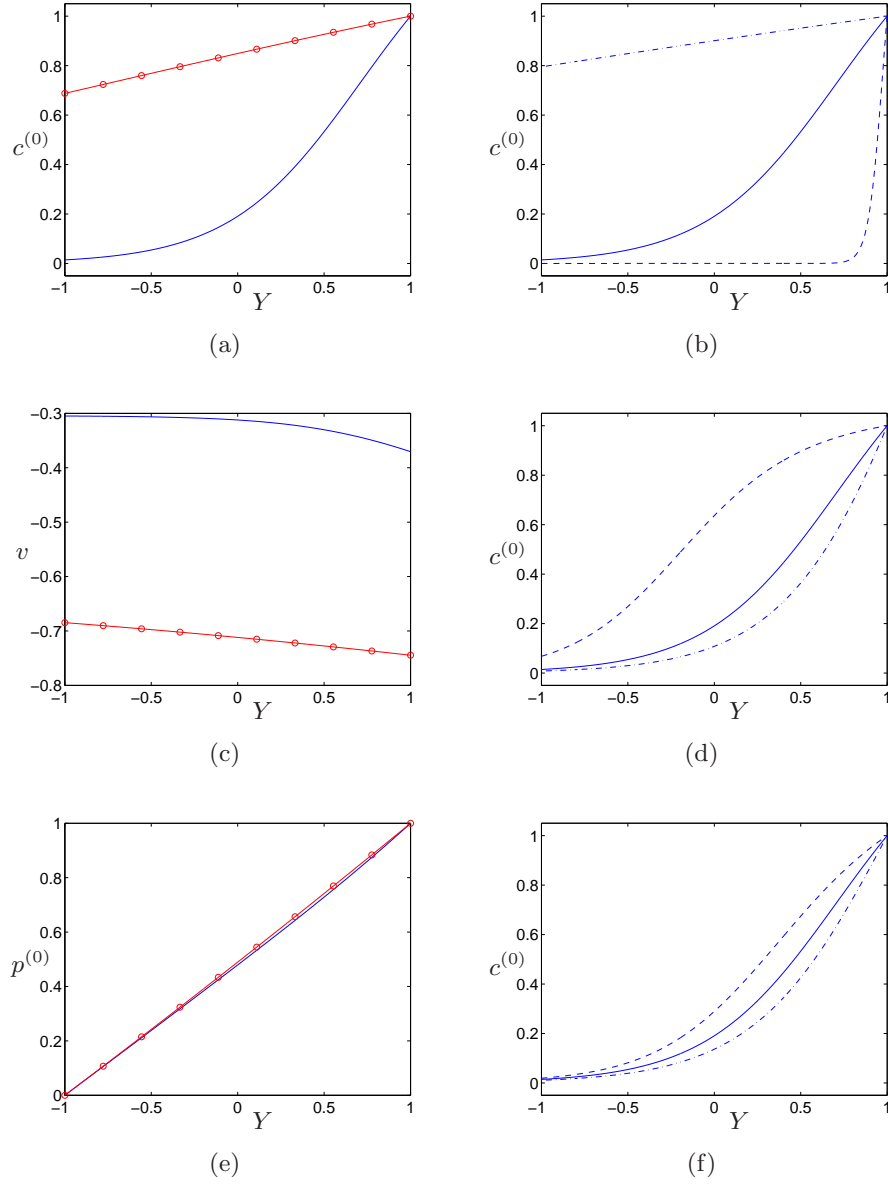


FIG. 5. Macroscale flow and transport profiles observed in numerical simulations of (3.25), (3.27), (3.29), (3.30), (4.2)–(4.4) at $t = 10$ and $X = 0$ (dimensionless units) within a PLLA scaffold of porosity $\Phi_f = 0.9$ ($\langle \mathbf{K}^{\mu CT} \rangle_f$; blue lines) or an array of circular obstructions ($\langle \mathbf{K}^\bullet \rangle_f$; red circles). (a,c,e) Nutrient concentrations $c^{(0)}$, axial fluid flow velocity (denoted v) and fluid pressure $p^{(0)}$. (b,d,f) Nutrient concentration profiles obtained for (b) $R = 0.1, 1, 10$, (d) $\alpha = 0.25, 0.5, 0.75$, (f) $\rho = 1, 1.25, 1.5$; in all cases, dot-dashed (resp. dashed) lines indicate the smallest (resp. largest) parameter choice. Unless otherwise stated $P_0 = C_0 = R = 1$, $\alpha = 0.5$, $\rho = 1.25$. Colour online.

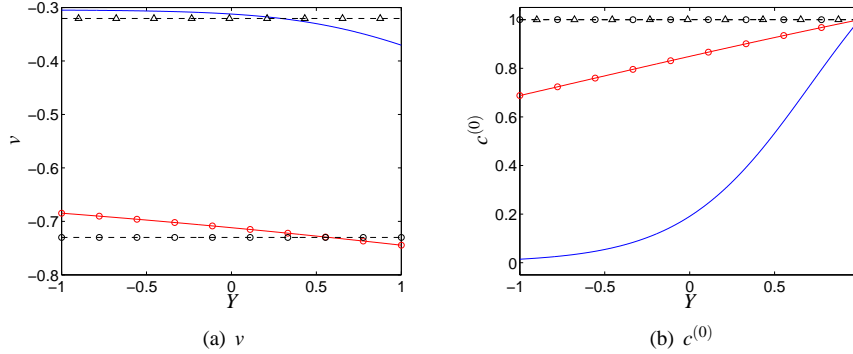


FIG. 6. Black dashed lines: numerical solutions of the macroscale model (3.25), (3.27), (3.29)–(4.4) showing (a) axial fluid flow velocity (denoted v), and (b) the macroscale nutrient distribution $c^{(0)}$ in the absence of growth ($R = 0$) for the PLLA scaffold ($\langle \mathbf{K}^{\mu CT} \rangle_f$; triangles) and for an array of circular obstructions ($\langle \mathbf{K}^\bullet \rangle_f$; circles). Red and blue lines show the corresponding results of Figures 5(a,b), with growth included. Except as indicated, $P_0 = C_0 = R = 1$, $\alpha = 0.5$, $\rho = 1.25$. Colour online.

constant flow, transporting nutrient from $Y = 1$ to $Y = -1$ via a travelling (discontinuous) wave connecting the state $c^{(0)} = 1$ to $c^{(0)} = 0$. This simple analysis emphasises the influence of microscale growth on the macroscale dynamics, and highlights the key role that balancing uptake associated with growth and advection has in controlling nutrient transport through the scaffold.

To summarise, in this section we have highlighted, via illustrative numerical simulations and simple analysis, that the microscale geometry of a growing porous structure influences significantly the flow, growth and transport dynamics and, moreover, that the inclusion of such growth leads to substantial differences in model dynamics in comparison to standard descriptions of flow in porous media. To effect this, we chose a computational domain inspired by applications in tissue engineering. Our results imply that the geometry of tissue engineering scaffolds (i) may influence significantly the microscale mechanical environment of the cells contained within them (via microscale flow and pressure variations) and (ii) may limit the effectiveness of perfusive bioreactors as nutrient delivery systems.

5. Discussion

In this paper, we have employed a multiple scales analysis to derive governing equations suitable to describe, at the macroscale, fluid flow and nutrient transport within a growing tissue, which nevertheless accommodate explicitly the influence of dynamics occurring at the microscale. The multiple scales technique that we employ has been widely applied in studies of porous and poroelastic materials (Burrige & Keller (1981), Mei & Auriault (1991) and many others); by incorporating microscale growth, we extend significantly the applicability of the method to biological problems. In particular, we analyse the process of appositional growth of a rigid porous material in response to its uptake of a generic diffusible nutrient, a behaviour of particular relevance to tissue growth and ECM deposition within appropriate tissue engineering scaffolds.

Our microscale model comprises a Newtonian fluid, which transports a passive diffusible solute, representing a generic nutrient, contained within a rigid porous material. We consider a representative microscale ‘pore’ (defined by a two-dimensional region $\mathbf{x} \in \Omega$), comprising both solid and fluid do-

mains; uptake of the solute by the solid component at the fluid–solid interface leads to tissue growth. We consider a simplified model for appositional growth, appropriate to the ‘thin-rim’ or ‘fast-consumption’ limit (King & Franks, 2007), in which such growth manifests itself as a change in position of the (non-material) solid–fluid interface, thereby altering the pore geometry. In this way, the flow, transport and growth dynamics are fully coupled at the microscale. Assuming that the micro- and macroscales are well-separated, we employ a multiple scales analysis to derive equations valid at the macroscale. The resulting model comprises a Darcy-type equation governing the flow of culture medium, coupled to an advection–reaction equation governing the transport of nutrient by the fluid and its uptake by the growing rim.

On the macroscale, the influence of the porous microstructure on the flow characteristics is evident via the permeability tensor, obtained via a well-known microscale Stokes flow problem. In this study, we demonstrate how tissue growth may be incorporated. As a consequence of the timescale on which we perform our analysis (and supported by the typical level of growth and mineralisation in relevant tissue engineering scaffolds) the microscale growth of the solid phase is relegated to $\mathcal{O}(\varepsilon)$, so that the leading order pore geometry is fixed. Nevertheless, our macroscale equations indicate that microscale growth influences directly the culture medium pressure. Therefore, in our macroscale representation, culture medium flow, nutrient transport and growth are fully coupled.

In addition to the development of new theoretical descriptions appropriate for growing tissues, a key aspect of the current study is the exposition by numerical simulation of our model’s predictions of macroscale flow, transport and growth dynamics within experimentally and biologically-relevant structures. As an illustrative example, we employ μ CT scans of a PLLA scaffold, used in a perfusion bioreactor system to develop bone tissue constructs, to define our periodic unit cell Ω . Numerical solution of the relevant Stokes cell problem indicates strong dependence of the microscale permeability \mathbf{K} and $\mathcal{O}(\varepsilon)$ pressure contribution on the underlying pore geometry. The strong local variations in these quantities are likely to lead to correspondingly large variations in microscale flow and transport characteristics, factors known to be of great importance in tissue growth phenomena. Indeed, the experimental studies on which we base our microscale domain (El Haj *et al.*, 1990; Baas *et al.*, 2010) considered explicitly the influence of flow-induced mechanical stimulation supplied to cells within such a scaffold. This microscale information is incorporated into the macroscale formulation via an anisotropic permeability tensor, and other coarse features of the microscale domain, such as its porosity and pore surface area. To highlight their influence on the macroscale dynamics, we obtain numerical solutions of the continuum equations corresponding to our representation of a two-dimensional PLLA scaffold, and compare them with those that arise when such a periodic microstructure is replaced by an array of circular obstructions. Our results indicate that the macroscale model incorporating growth that we derive leads to substantial differences in system dynamics, in comparison to standard descriptions of flow and transport in porous media, and that a complex microstructure, such as that of the PLLA scaffold, leads to a marked reduction in axial nutrient transport. The differences in flow and transport dynamics between the two microstructures arise due to a significantly larger interfacial domain in the PLLA scaffold, leading to increased nutrient uptake; the growth associated with such uptake generates further flow restriction, and enhanced nutrient uptake. Our simulations indicate that, after an initial period in which nutrient spreads into the domain from the source point, the distributions evolve to steady spatially-varying configurations from which further spreading is minimal for large times, due to a balance between uptake associated with growth, and transport. Therefore, scaffold regions which are distant from the nutrient source are starved of nutrient for the duration of the culture period, and exhibit very low growth.

In summary, we have indicated that current multiscale homogenisation approaches may be extended to accommodate microscale growth in a rigorous way. Further, the numerical results that we have pre-

sented illustrate that, together with growth, a complex microstructure of the type illustrated in Figure 2 leads to altered microscale flow patterns and significantly restricted macroscale flow and nutrient transport in tissue engineering scaffolds. Our analysis suggests that a careful balance between cellular uptake, scaffold microstructure and perfusion velocity is required in order to deliver effectively nutrient to the entire scaffold. Our interest here is in the development of new theoretical models and the illustration of possible model behaviour via numerical simulation and so we neither consider matching to experimental data via appropriate parameter estimation, nor a detailed parameter study, both of which form important future work.

While the assumption of microscale periodicity that underpins the two-scale homogenisation method may not apply to all tissues, within *in vitro* tissue engineering applications, scaffold manufacture can be controlled via advanced production techniques to obtain a highly regular microstructure. This study indicates how experimental imaging data may be accommodated within such formulations – the majority of studies in this area deal exclusively with theoretical model development. The assumption of local periodicity is partially ameliorated by noting that our formulation accommodates macroscale variation in the geometry of Ω ; the reader interested in the application of the homogenisation method to more disordered media is directed to Chernyavsky *et al.* (2011) and references therein.

We have considered a rigid porous material, and analysed the process of surface accretion in response to local nutrient concentration, modelled by a simple mass-jump condition which is applied at a non-material interface. A recent related study (Penta *et al.*, 2014) considers a deformable (linear-elastic) substrate (the resulting model describes a nutrient-independent growth of a *poroelastic* material); natural extensions of the current work include consideration of nutrient-limited poroelastic growth, and the inclusion of the influence of the microscale mechanical environment on tissue growth – the latter are known to be crucial to the development of viable tissue constructs suitable for implantation and may be incorporated by a suitable functional dependence of the interfacial growth term $S^{(1)}$ on, *e.g.*, the shear stress exerted by the fluid on the fluid–solid interface. An additional area of future work is to obtain, via the methods herein, a macroscale model which includes interstitial growth (in which growth, deformation and remodelling occur throughout the tissue domain). The latter presents significant mathematical challenges, such as obtaining an appropriate representation of growth-induced residual stresses; however, such a formulation will be applicable in the modelling of a wide range of biological phenomena and is therefore important future work.

6. Acknowledgements

This publication was based on work supported in part by Award No. KUK-C1-013-04, made by King Abdullah University of Science and Technology (KAUST). We thank E. Baas, (ISTM, Keele University) for the provision of experimental data. We acknowledge helpful contributions from J.R. King, and also thank R. Penta, R.J. Shipley and D. Ambrosi. Lastly, we thank the anonymous reviewers for their helpful suggestions.

References

- Ambrosi, D. , Preziosi, L. and Vitale, G. , 2010. The insight of mixtures theory for growth and remodeling. *Zeitschrift für angewandte Mathematik und Physik (ZAMP)*, 61(1):177–191.
- Araujo, R.P. and McElwain, D.L.S , 2005. A mixture theory for the genesis of residual stresses in growing tissues I: A general formulation. *SIAM J. of App. Math.*, 65(4):1261–1284.

- Ateshian, G.A. , 2011. The role of mass balance equations in growth mechanics illustrated in surface and volume dissolution. *J. Biomech. Eng.*, 133(1):011010.
- Baas, E. , Kuiper, J.H. , Yang, Y. , Wood, M.A. and El Haj, A.J. , 2010. In vitro bone growth responds to local mechanical strain in three-dimensional polymer scaffolds. *J. Biomech.*, 43(4):733–739.
- Band, L.R. and King, J.R. , 2012. Multiscale modelling of auxin transport in the plant-root elongation zone. *Journal of mathematical biology*, 65(4):743–785.
- Bathe, M. , Shirai, A. , Doerschuk, C. M and Kamm, R. D. , 2002. Neutrophil transit times through pulmonary capillaries: the effects of capillary geometry and fmlp-stimulation. *Biophys. J.*, 83(4): 1917–1933.
- Bridge, L.J. , King, J.R. , Hill, S.J. and Owen, M.R. , 2010. Mathematical modelling of signalling in a two-ligand g-protein coupled receptor system: Agonist–antagonist competition. *Math. Biosci.*, 223 (2):115–132.
- Burridge, R. and Keller, J.B. , 1981. Poroelasticity equations derived from microstructure. *J. Acous. Soc. Am.*, 70:1140.
- Chapman, S.J. , Shipley, R.J. and Jawad, R. , 2008. Multiscale modeling of fluid transport in tumors. *Bull. Math. Biol.*, 70(8):2334–2357.
- Chavarría-Krauser, A. and Ptashnyk, M. , 2010. Homogenization of long-range auxin transport in plant tissues. *Nonlinear Analysis: Real World Applications*, 11(6):4524–4532.
- Chernyavsky, I.L. , Leach, L. , Dryden, I.L. and Jensen, O.E. , 2011. Transport in the placenta: homogenizing haemodynamics in a disordered medium. *Phil. Trans. R. Soc. A*, 369(1954):4162–4182.
- Collier, J.R. , Monk, N.A.M. , Maini, P.K. and Lewis, J.H. , 1996. Pattern Formation by Lateral Inhibition with Feedback: a Mathematical Model of Delta-Notch Intercellular Signalling. *J. Theor. Biol.*, 183(4):429–446.
- Dervaux, J. and Ben Amar, M. , 2008. Morphogenesis of growing soft tissues. *Phys. Rev. Lett.*, 101: 068101 (4pp).
- Dervaux, J. and Ben Amar, M. , 2010. Localized growth of layered tissues. *IMA J. Appl. Math.*, 75: 571–580.
- El Haj, A.J. , Minter, S.L. , Rawlinson, S.C. , Suswillo, R. and Lanyon, L.E. , 1990. Cellular responses to mechanical loading in vitro. *J. Bone and Min. Res.*, 5(9):923–32.
- Fozard, J.A. , Byrne, H.M. , Jensen, O.E. and King, J.R. , 2010. Continuum approximations of individual-based models for epithelial monolayers. *Math. Med. Biol.*, 27(1):39–74.
- Freed, L.E. , Vunjak-Novakovic, G. , Biron, R.J. , Eagles, D.B. , Lesnoy, D.C. , Barlow, S.K. and Langer, R. , 1994. Biodegradable polymer scaffolds for tissue engineering. *Nat. Biotech.*, 12(7):689–693.
- Hollister, S.J. , 2005. Porous scaffold design for tissue engineering. *Nature Mat.*, 4(7):518–524.
- Horch, R.E. , Kopp, J. , Kneser, U. , Beier, J. and Bach, A.D. , 2007. Tissue engineering of cultured skin substitutes. *J. Cell. Mol. Med.*, 9(3):592–608.

- Humphrey, J.D. , 2003. Review paper: Continuum biomechanics of soft biological tissues. *Proceedings of the Royal Society of London. Series A: Mathematical, Physical and Engineering Sciences*, 459 (2029):3–46.
- Hutmacher, D.W. , Sittinger, M. and Risbud, M.V. , 2004. Scaffold-based tissue engineering: rationale for computer-aided design and solid free-form fabrication systems. *Trends Biotechnol.*, 22(7):354–362.
- King, J.R. and Franks, S.J. , 2007. Mathematical modelling of nutrient-limited tissue growth. In *Free Boundary Problems*, pages 273–282. Springer.
- Lemon, G. , King, J.R. , Byrne, H.M. , Jensen, O.E. and Shakesheff, K. , 2006. Multiphase modelling of tissue growth using the theory of mixtures. *J. Math. Biol.*, 52(2):571–594.
- Mack, P.J. , Kaazempur-Mofrad, M.R. , Karcher, H. , Lee, R.T. and Kamm, R.D. , 2004. Force-induced focal adhesion translocation: effects of force amplitude and frequency. *Am. J. Physiol. - Cell Ph.*, 287 (4):C954–C962.
- Marciniak-Czochra, A. and Ptashnyk, M. , 2008. Derivation of a macroscopic receptor-based model using homogenization techniques. *SIAM Journal on Mathematical Analysis*, 40(1):215–237.
- Mei, C.C. and Auriault, J.L. , 1991. The effect of weak inertia on flow through a porous medium. *J. Fluid Mech.*, 222(1):647–663.
- Meineke, F.A. , Potten, C. S. and Loeffler, M. , 2001. Cell migration and organization in the intestinal crypt using a lattice-free model. *Cell Prolif.*, 34(4):253–266.
- Mikos, A.G. , Thorsen, A.J. , Czerwonka, L.A. , Bao, Y. , Langer, R. , Winslow, D.N. and Vacanti, J.P. , 1994. Preparation and characterization of poly (l-lactic acid) foams. *Polymer*, 35(5):1068–1077.
- Nelson, M.R. , Howard, D. , Jensen, O.E. , King, J.R. , Rose, F.R.A.J. and Waters, S.L. , 2011. Growth-induced buckling of an epithelial layer. *Biomech. Mod. Mechanobiol.*, 10(6):883–900.
- Nelson, M.R. , King, J.R. and Jensen, O.E. , 2013. Buckling of a growing tissue and the emergence of two-dimensional patterns. *Mathematical biosciences*, 246(2):229–241.
- O’Dea, R.D. and King, J.R. , 2011. Multiscale analysis of pattern formation via intercellular signalling. *Math. Biosci.*, 231:172–185.
- O’Dea, R.D. and King, J.R. , 2012. Continuum limits of pattern formation in hexagonal-cell monolayers. *J. Math. Biol.*, 64:579–610.
- O’Dea, R.D. , Waters, S.L. and Byrne, H.M. , 2010. A multiphase model for tissue construct growth in a perfusion bioreactor. *Math. Med. Biol.*, 27(2):95–127.
- Penta, R. , Ambrosi, D. and Shipley, R.J. , 2014. Effective governing equations for poroelastic growing media. *Q. J. Mech. Appl. Math.*, 67(1):69–91.
- Ptashnyk, M. and Roose, T. , 2010. Derivation of a macroscopic model for transport of strongly sorbed solutes in the soil using homogenization theory. *SIAM Journal on Applied Mathematics*, 70(7):2097–2118.

- Rubinstein, J. and Torquato, S. , 1989. Flow in random porous media: mathematical formulation, variational principles, and rigorous bounds. *J. Fluid Mech.*, 206:25–46.
- Shipley, R.J. . 2008. *Multiscale Modelling of Fluid and Drug Transport in Vascular Tumours*. PhD thesis, University of Oxford, UK.
- Shipley, R.J. and Chapman, S.J. , 2010. Multiscale modelling of fluid and drug transport in vascular tumours. *Bull. Math. Biol.*, 72(6):1464–1491.
- Turner, S. , Sherratt, J.A. , Painter, K.J. and Savill, N.J. , 2004. From a discrete to a continuous model of biological cell movement. *Phys. Rev. E*, 69(2):21910/1–21910/10.
- Van Leeuwen, I.M.M. , Mirams, G. R. , Walter, A. , Fletcher, A. , Murray, P. , Osborne, J. , Varma, S. , Young, S. J. , Cooper, J. , Doyle, B. *et al.*, 2009. An integrative computational model for intestinal tissue renewal. *Cell proliferation*, 42(5):617–636.
- Webb, S.D. and Owen, M.R. , 2004. Intra-membrane ligand diffusion and cell shape modulate juxtacrine patterning. *J. Theor. Biol.*, 230(1):99–117.
- Zick, A.A. and Homsy, G.M. , 1982. Stokes flow through periodic arrays of spheres. *J. Fluid Mech.*, 115(1):13–26.